

Article

Geometric, Electronic, and Optoelectronic Properties of Carbon-Based Polynuclear $C_3O[C(CN)_2]_2M_3$ (where $M = Li, Na,$ and K) Clusters: A DFT Study

Imene Bayach ^{1,*}, Atazaz Ahsin ^{2,†}, Safi Ullah Majid ², Umer Rashid ², Nadeem S. Sheikh ³  and Khurshid Ayub ^{2,*}

¹ Department of Chemistry, College of Science, King Faisal University, Al-Ahsa 31982, Saudi Arabia

² Department of Chemistry, Abbottabad Campus, COMSATS University Islamabad, Abbottabad 22060, KPK, Pakistan

³ Chemical Sciences, Faculty of Science, University Brunei Darussalam, Jalan Tungku Link, Gadong BE1410, Brunei Darussalam

* Correspondence: ibayach@kfu.edu.sa (I.B.); khurshid@cuiatd.edu.pk (K.A.)

† These authors contributed equally to this work.

Abstract: Carbon-based polynuclear clusters are designed and investigated for geometric, electronic, and nonlinear optical (NLO) properties at the CAM-B3LYP/6-311++G(d,p) level of theory. Significant binding energies per atom (ranging from -162.4 to -160.0 kcal mol⁻¹) indicate excellent thermodynamic stabilities of these polynuclear clusters. The frontier molecular orbital (FMOs) analysis indicates excess electron nature of the clusters with low ionization potential, suggesting that they are alkali-like. The decreased energy gaps (E_{H-L}) with increased alkali metals size reveal the improved electrical conductivity (σ). The total density of state (TDOS) study reveals the alkali metals' size-dependent electronic and conductive properties. The significant first and second hyperpolarizabilities are observed up to 5.78×10^3 and 5.55×10^6 au, respectively. The β_o response shows dependence on the size of alkali metals. Furthermore, the absorption study shows transparency of these clusters in the deep-UV, and absorptions are observed at longer wavelengths (redshifted). The optical gaps from TD-DFT are considerably smaller than those of HOMO-LUMO gaps. The significant scattering hyperpolarizability (β_{HRS}) value (1.62×10^4) is calculated for the C3 cluster, where octupolar contribution to β_{HRS} is 92%. The dynamic first hyperpolarizability $\beta(\omega)$ is more pronounced for the EOPE effect at 532 nm, whereas SHG has notable values for second hyperpolarizability $\gamma(\omega)$.

Keywords: polynuclear superalkali clusters; excess electrons; nonlinear optical response; dynamic hyperpolarizability



Citation: Bayach, I.; Ahsin, A.; Majid, S.U.; Rashid, U.; Sheikh, N.S.; Ayub, K. Geometric, Electronic, and Optoelectronic Properties of Carbon-Based Polynuclear $C_3O[C(CN)_2]_2M_3$ (where $M = Li, Na,$ and K) Clusters: A DFT Study. *Molecules* **2023**, *28*, 1827. <https://doi.org/10.3390/molecules28041827>

Academic Editors: Pratim Kumar Chattaraj, Sudip Pan and Debdutta Chakraborty

Received: 31 December 2022

Revised: 5 February 2023

Accepted: 6 February 2023

Published: 15 February 2023



Copyright: © 2023 by the authors. Licensee MDPI, Basel, Switzerland. This article is an open access article distributed under the terms and conditions of the Creative Commons Attribution (CC BY) license (<https://creativecommons.org/licenses/by/4.0/>).

1. Introduction

Nonlinear optical (NLO) materials are at the front line of research in interdisciplinary science and laser-based technology due to their fundamental applications in the field of optoelectronics [1–4]. Photonic devices, laser-based technology, endoscope, and sensors are examples of well known technologies where NLO materials have possible applications [5–12]. To design and synthesize the NLO materials, much efforts are exerted to understand the origin of nonlinearity in molecules and clusters in order to correlate NLO responses to electronic structure and molecular geometry. Polarization, asymmetric charge distribution, asymmetric crystal packing, and π -conjugated electron transport routes are all required for NLO materials. Because of their high thermal stability and transparency, inorganic nonlinear optical materials have been preferred over organic ones [13]. Some inorganic borates crystals, such as KB₅ (KB₅O₈H₂O), BBO (-BaB₂O₄), and LiB₃O₅ (LBO), have been investigated as good NLO materials, particularly in the ultraviolet range [13].

For obtaining high-performance NLO materials, several strategies were proposed, which include bond length alternation (BLA) [14], doping metal atoms [15], push–pull

mechanisms from donor to acceptor [16], modification of sp^2 hybridized carbon nanomaterials [17], designing octupolar molecules [18], multidecker sandwich complexes [19], and excess electron induction [20].

The introduction of excess electrons into molecules and clusters is the most viable technique to escalate hyperpolarizability. The availability of loosely bound electrons predominantly decreases the excitation energies for the crucial transition [21–23]. Excess electrons in molecules and crystals behave similarly to Rydberg orbitals, which are positioned outside the parent molecules and are held loosely [24–26]. Several studies have demonstrated the substantial role of the diffuse excess electrons in compounds for developing NLO materials. Wei Chen et al. investigated the Li@calix[4]pyrrole electrone complex, which has a significant static hyperpolarizability (β_o) value of up to 7.3×10^3 au, where the presence of excess electrons has a significant role [27].

Theoretically designed compounds having excess electrons that are further classified into [28] alkalides [29], alkaline-earthides [30], metalides [31], and electrides [32]. Alkalides are complex compounds in which alkali metals bear the negative charge (Li^- , Na^- , K^-) [33]. On the other hand, electride complexes have anionic sites occupied by the electron inside the complexes [34]. Furthermore, the alkaline-earthides were recently introduced to excess electrons compounds, where the alkaline earth metals hold a negative charge [35]. Interestingly, superalkali clusters are a new class of materials that can transport electrons, making them useful for the fabrication of electro-optical materials [36].

Superalkali clusters with lower ionization energy (IE) than alkali metal elements are well known due to their powerful reducing capabilities. The very first report about superalkali was obtained in 1982 by Gutsev and Boldyrev for Li_3O , Li_2F , and Li_4N clusters [37]. These clusters with unique qualities, such as tuneability in their electrical properties and the ability to function as a bridge between micro and macro materials, are of great interest to cluster science. Recent advances in cluster science show the potential applications of superalkali clusters, i.e., the reductive materials, helium and hydrogen storage, catalysis, supersalt formation, and nonlinear optics [38–41].

Superalkali clusters are excellent candidates for creating optical and NLO materials because of their excellent tunable electronic and structural properties. The decreased excitation energy may be responsible for electrons shifting from HOMO to LUMO, as they are loosely bound. Based on the intriguing characteristics of superalkali clusters, these were used to fabricate NLO materials. In this regard, two-dimensional materials doped superalkali, and they play an essential role in triggering the hyperpolarizability response. Sun et al. theoretically designed superalkali-based alkalides $Li_3^+(\text{calix}[4]\text{pyrrole})M^-$, $Li_3O^+(\text{calix}[4]\text{pyrrole})M^-$, and $M_3O^+(\text{calix}[4]\text{pyrrole})K^-$ ($M = Li, Na, \text{ and } K$), where the hyperpolarizability response is recorded up to 34718 au [42]. Similarly, Faizan Ullah et al. reported a noticeable enhancement in the NLO response of the $A_{12}P_{12}$ nanocluster by using Li_4N , Li_2F , and Li_3O superalkalis as the source of the excess electrons [43]. Furthermore, macrocyclic oligofurans ring doped with superalkali clusters were also reported as a new kind of nonlinear optical material where a larger hyperpolarizability response is attributed to the presence of loosely bound electrons [44].

Although a larger number of superalkali clusters were theoretically designed, very limited studies have been conducted to show the possibility of using polynuclear superalkali (undoped) clusters as NLO materials. Srivastava et al. investigated the electronic and nonlinear optical properties Li_nF ($n = 2-5$) and M_2X small clusters as excess electron compounds where the β_o increases up to 10^5 au for Li_2F [45,46]. Our group investigated the static and dynamic hyperpolarizability response of M_2OCN and M_2NCO ($M = Li, Na, K$) superalkali clusters as excess electrons candidates where the second hyperpolarizability $\gamma(\omega)$ values were calculated up to 2.1×10^8 au [45].

Superalkali clusters can be mononuclear, bimetallic, and polynuclear based on their rational design and elemental composition. We are interested to investigate carbon-based polynuclear clusters for electronic and NLO properties. These clusters are more stable than conventional mononuclear superalkali clusters and might possess better electronic and

NLO properties. The previous development in the family of superalkalis and their tunable electronic properties prompted us to further investigate polynuclear clusters for optical and NLO properties. Polynuclear carbon-based clusters $C_3O[C(CN)_2]_2M_3$ (where $M = Li, Na, \text{ and } K$) are investigated using DFT.

2. Results and Discussion

2.1. Optimized Geometries and Thermodynamic Stabilities

The optimized geometries of carbon-based polynuclear superalkali clusters $C_3O[C(CN)_2]_2M_3$ (where $M = Li, Na, \text{ and } K$) optimized at CAM-B3LYP/6-311++g(d,p) are given in Figure 1. The studied polynuclear structures (**C1** to **C3**) show C_{2V} point group symmetry (Table 1). These clusters are planar with a central carbon core. The determined bond distances between alkali metal and oxygen (d_{M-O}) are in increasing fashion with the increased size of metals (Li to K). The calculated d_{M-O} bond distances for **C1**, **C2**, and **C3** are 1.82, 2.24, and 2.58 Å, respectively (Table 1). The observed geometric parameters (Supplementary Materials) are very consistent with the previously reported study in the literature. Furthermore, these polynuclear clusters also show the increased bond distance between metals and nitrogen (d_{M-N}). The observed bond lengths (d_{M-N}) are 1.89, 2.26, and 2.62 Å for **C1**, **C2**, and **C3** clusters. The observed monotonic increase in bond lengths from Li to K may be attributed to increased metal size. The performed frequency calculation shows that there is no imaginary frequency associated with these clusters, and these are true minima on the potential energy surface.

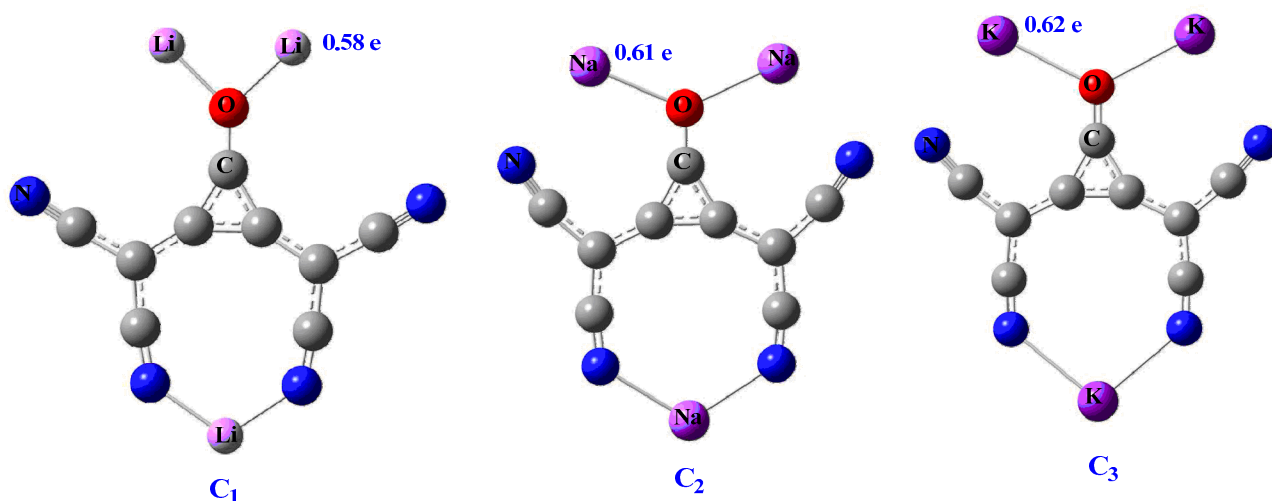


Figure 1. Optimized structure of Clusters **C1** to **C3**.

Table 1. Computed bond length between metal and O-atom (d_{M-O} in Å), the bond length between alkali metals and N-atom (d_{M-N} in Å), binding energies per atom (E_b in kcal mol⁻¹), NBO charges on metals (QM), NBO charge on nitrogen (QN), NBO charge on oxygen atom (QO), VIE (in eV), and VEA (in eV), of **C1** to **C3** clusters.

Cluster	d_{M-O}	d_{M-N}	E_b	Q(M)	Q(N)	Q(O)	VIE	VEA
C1	1.82	1.89	-162.4	0.58	-0.485	-0.960	3.65	0.76
C2	2.24	2.26	-160.1	0.61	-0.521	-0.839	3.41	0.89
C3	2.58	2.62	-162.1	0.62	-0.523	-0.830	3.00	0.27

The thermodynamic stability of the studied polynuclear clusters is evaluated through calculated binding energy per atom (E_b). Overall, the binding energies range from -160.1 to -162.1 kcal mol⁻¹ (Table 1), where the highest energy is found for **C1**, while the lowest is observed for the **C2** cluster. The obtained significant binding energies per atom suggests

their thermodynamic stabilities. The calculated binding energies are higher in comparison to previously reported superalkali clusters $NM'M$ (where $M = \text{Li, Na and K}$), $C_3X_3Y_3$ ($X = \text{O, S, and } Y = \text{Li, Na and K}$) and bimetallic superalkali clusters [47,48]. The trend of binding energies per atom for studied clusters is also shown in Figure 2. Compared to clusters **C2** and **C3**, cluster **C1** has a greater binding energy value. The computed binding energies show high thermal stability of these clusters, which demonstrate that they can be synthesized experimentally.

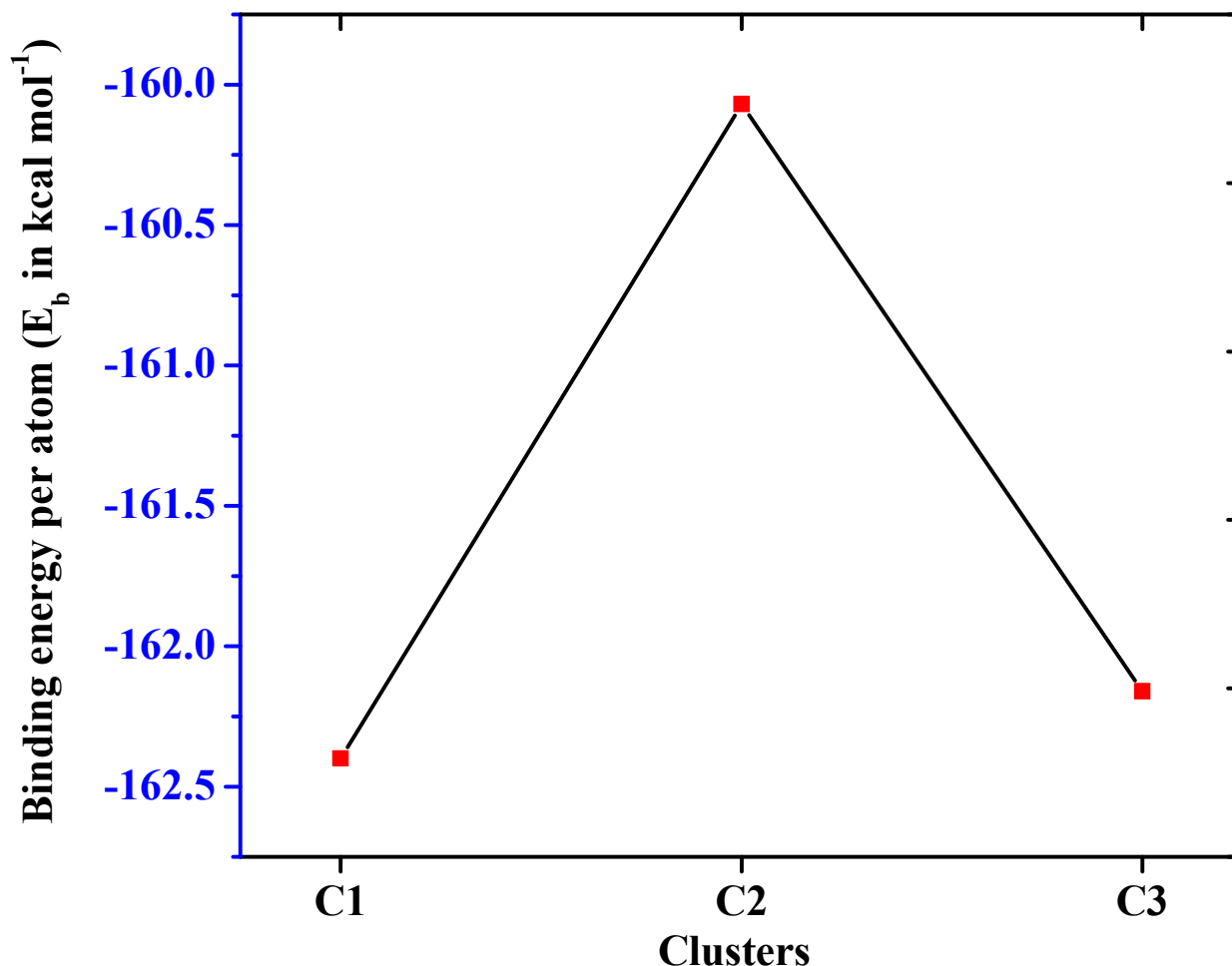


Figure 2. Binding energies per atom (E_b) of clusters.

2.2. Electronic Properties and Stability

The electronic stability and superalkali nature of these clusters can be observed from calculated ionization potential and electron affinity. The obtained vertical ionization potential values are smaller than Cs-atom (3.89 eV), which shows the superalkali characteristics of these clusters. These values are also significant and account for the electronic stabilities of these clusters. The highest VIE value of 3.65 eV is found for **C1**, while the lowest value (3.0 eV) is indicated for the **C3** cluster (Table 1). A gradual decrease in VIE values with the increased size of alkali metals can be seen in these clusters. On the other hand, the vertical electron affinity (VEA) values range from 0.27 to 0.89 eV, where **C3** shows the lowest value. The reduced values of EA indicate the electropositive nature of these clusters.

To obtain reactivity and charge distribution, the computed NBO charges are given in Table 1. The NBO charges (positive) on alkali metals slightly increase from Li to K metals. The charge is transferred from alkali metals to electronegative atoms (oxygen and nitrogen) within clusters. The NBO charges on alkali metals (QM) lie in the range of 0.58 to 0.62 e, where **C1** shows higher charge (positive magnitude) on metals. The charge transferred

from alkali to O-atom is more pronounced as compared to the alkali to N-atom transition, which may be attributed to the higher electronegativity of the oxygen atom. The calculated NBO charges on O-atom (QO) lie in the range of -0.83 to -0.96 e and are higher for small-sized metals.

2.3. Global Reactivity Descriptor

To characterize the reactivity of these clusters, we calculated global reactivity descriptor, chemical hardness, softness, and chemical potential (Table 2). The chemical hardness is measured as resistance to change in electronic distribution within clusters. The results obtained show that the C3 cluster has the highest value (1.839 eV) of hardness, whereas the C1 has the lowest value. The size of alkali metals is an obvious factor in controlling the hardness of clusters. The decreased values show a correlation with increased atomic size (Li to K), which guarantees soft nature and reactivity (Table 2). Similarly, the values of chemical softness (S) increase from C1 to C3 and reach the maximum of 0.33 eV.

Table 2. Energies of HOMO (E_{HOMO} in eV), LUMO energies (in eV), HOMO-LUMO gaps ($E_{\text{H-L}}$ in eV), chemical hardness (η in eV), chemical softness (S in eV), chemical potential (χ in eV), oscillator strength (f_o in au), excitation energies (eV), and maximum absorption (in nm) of C1 to C3 clusters.

Cluster	E_{HOMO}	E_{LUMO}	$E_{\text{H-L}}$	η	S	χ
C1	-4.70	-0.61	4.08	1.839	0.27	-1.81
C2	-3.24	-0.88	2.35	1.721	0.29	-1.72
C3	-2.80	-0.83	1.96	1.505	0.33	-1.50

The chemical potential values are also calculated and given in Table 2. The higher chemical potential (χ) values show the escaping tendency of the electrons in clusters and molecules. Obtained significant values (negative) indicate the stability of these polynuclear clusters. These values also suggest that the clusters do not decompose spontaneously into atoms and possess reasonable electronic stability.

2.4. FMO Analysis and Excess Electron Nature of Clusters

To provide deep insight into the electronic structures of the studied clusters, the densities of the highest occupied molecular orbitals (HOMO) and virtual orbitals are plotted, and their energy values are given in Table 2. The HOMO and LUMO are quite important in quantum chemistry, as they allow the prediction of chemical stability and reactivity of molecules. Imperatively, the small difference between HOMO-LUMO ($E_{\text{H-L}}$) is crucial for the description of reactivity of molecules. The smaller $E_{\text{H-L}}$ gaps depict greater chemical reactivity with a high tendency to be polarized, as well as low kinetic stability. The HOMO-LUMO gap values lie in the range of 4.08 to 1.96 eV, where the highest value corresponds to C1 clusters, while the lowest values correspond for C3. One can note that $E_{\text{H-L}}$ decreases with increased metals size (Li to K) within clusters. Furthermore, decreased $E_{\text{H-L}}$ gaps for the studied clusters can be attributed to increased energies of occupied orbitals where the energy of virtual orbitals goes on decreasing.

The reactivity and conducting qualities of these clusters are revealed by a significant reduction in HOMO-LUMO gaps; there are excitable valence electrons (excess electrons) with transition HOMO \rightarrow LUMO. The excess electron nature is further justified by the distribution of HOMO densities, and the electronic density cloud is mainly spread over alkali metals, which indicates the excess electron character of these superalkali clusters. The three-dimensional HOMO density of C1 is shaped as a s-orbital, while for C2 and C3, its look like a diffuse p-orbital (Figure 3). The LUMO densities that are generated are spherical and resemble s-orbitals.

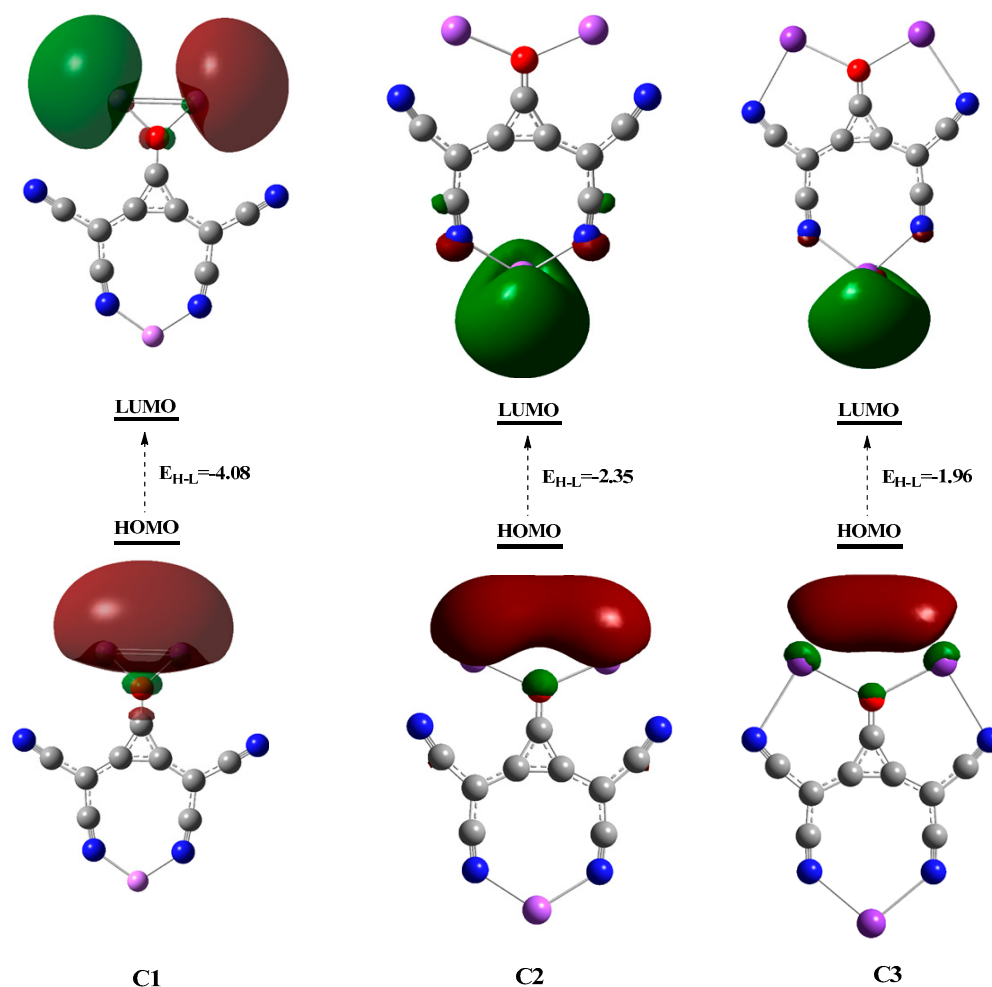


Figure 3. Generated HOMO and LUMO densities of clusters.

2.5. Electrical Conductivity (σ)

The electrical conductivity is also a crucial aspect to demonstrate the NLO properties of molecules. The electrical conductivity (σ) is the function of energy gaps (E_{H-L}); thus, narrowing HOMO-LUMO gaps more will lead to higher electrical conductivity of materials. In our designed clusters, the HOMO-LUMO gaps are significantly reduced from 4.08 to 1.96 eV. The electrical conductivity increases with increased size of alkali metals, which might be attributed to ease in excitation of electrons (HOMO to LUMO).

2.6. TD-DFT Analysis

In the transparent region, the applications of nonlinear optical materials can be better understood. The obtained TD-DFT parameters of crucial transitions and first allowed transitions are given in Table 3. The percentage contribution of particular orbitals of these clusters for both transitions are also given in Table 3, whereas spectra are shown in Figure 4. The higher value of ϵ shows strong absorption at particular wavelength. Additionally, a higher value of f_o reveals the strong transition probability. The studied cluster C3 has significant value of ϵ and oscillator strength at higher wavelength. The absorption maxima (λ_{max}) during crucial transition for C1, C2, and C3 are 758, 688, and 995 nm, respectively, where the redshifted (i.e., bathochromic shift) in λ_{max} is observed for C3 (Table 3). The obtained excitation energies of crucial transition are 1.63, 0.92, and 1.24 eV for C1, C2, and C3 clusters. On the other hand, the obtained optical gaps during allowed transitions are 1.63, 0.92, and 0.86 eV. The C1 cluster has same value for crucial excitation and optical gap, while for C2 and C3, optical gaps (allowed transition) values are significantly reduced. The excitation energies of allowed transition are decreasing monotonically from C1 to C3

with increased metal size (Li to K). The absorption maxima (λ_{\max}) of allowed transition are observed at longer wavelength as compared to absorption during crucial transition. As a result, bigger alkali metals have a stronger influence on absorptions shift to higher wavelengths. Furthermore, these clusters are completely transparent under the deep-UV region and have broadband absorption in the near-Visible region (Figure 4). The highest energy state TD-DFT parameters also reveal transparency in the deep-UV region, while absorption is mostly in the UV-visible region (Table 3). Likewise, the gradual increase in oscillator strength (f_o) can also be seen for C1 to C3 clusters for crucial transition and allowed transition, which suggest increased quantum chemical excitation probabilities in higher-sized clusters.

Table 3. TD-DFT parameters of crucial excited states, first allowed transitions, and highest state for C1 to C3 clusters.

Clusters	TD-DFT Parameters from Crucial Transitions			
	ΔE (eV)	λ_{\max} (nm)	f_o (au)	Major Orbital Contribution
C1	1.63	758	0.19	HOMO→LUMO+2 (82%)
C2	1.80	688	0.26	HOMO→LUMO+3 (36%)
C3	1.24	995	0.28	HOMO→LUMO+5 (67%)
TD-DFT Parameters from First Allowed Transitions				
C1	1.63	758	0.19	HOMO→LUMO+2 (82%)
C2	0.92	1338	0.23	HOMO→LUMO+1 (99%)
C3	0.86	1441	0.25	HOMO→LUMO+1 (96%)
TD-DFT Parameters for Highest Energy States				
C1	5.12	242		0.0018
C2	4.25	291		0.0005
C3	3.92	315		0.0002

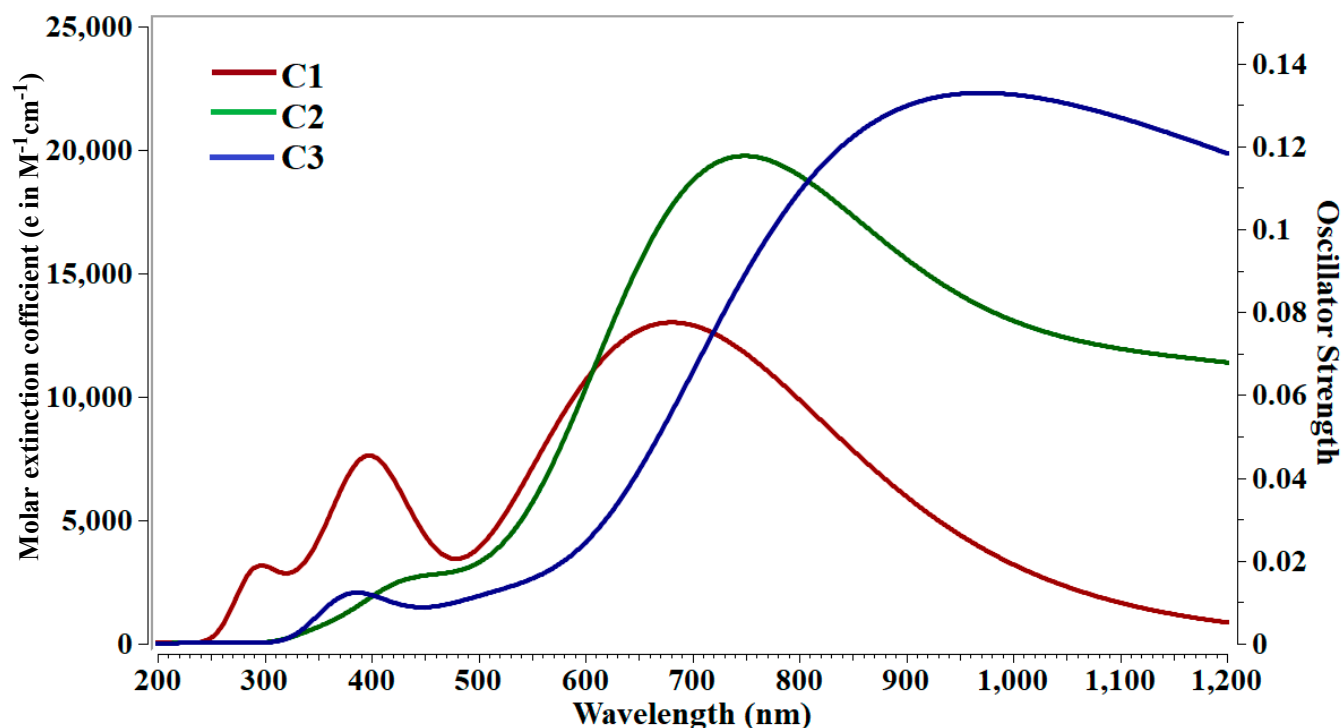


Figure 4. Absorption spectra of C1 to C3 clusters.

2.7. Dipole Moment (μ_o) and Change in Dipole Moment ($\Delta\mu$)

For better comprehension of the electronic properties in these clusters, the dipole moment (μ_o) and change in dipole moments ($\Delta\mu$) values are also calculated. Overall, the dipole moment and change in dipole moment ($\Delta\mu$) values are quite significant, which reveal asymmetric electronic distribution in these clusters (Table 4). The measured total dipole moment indicate polarity in clusters and the values of μ_o are significant and range from 1.49 to 4.11 au, where the highest value is observed for the **C3** cluster. On the other hand, the total change in dipole moment ($\Delta\mu$) values are slightly smaller than those of dipole moment, but **C2** shows a significant value of 4.69 au (Table 4).

Table 4. Polarizabilities (α_o in au), hyperpolarizabilities (β_o in au), second hyperpolarizability (γ_o in au), scattering hyperpolarizability (β_{HRS} in au), vector part of hyperpolarizability (β_{vec} in au), average hyperpolarizability ($\langle\beta_{j=1}\rangle$ in au), average octupolar hyperpolarizability ($\langle\beta_{j=3}\rangle$ in au), % dipolar contribution to hyperpolarizability $\Phi\beta(j=1)$, and % octupolar contribution to hyperpolarizability $\Phi\beta(j=3)$ of C1 to C3 clusters.

Clusters	α_o	β_o	γ_o	β_{HRS}	β_{vec}	$\langle\beta_{j=1}\rangle$	$\langle\beta_{j=3}\rangle$	$\Phi\beta(j=1)$	$\Phi\beta(j=3)$
C1	2.5×10^2	2.37×10^3	5.5×10^6	1.34×10^3	2.37×10^3	1.8×10^3	3.37×10^3	35%	65%
C2	5.07×10^2	4.46×10^3	1.2×10^6	4.87×10^3	4.46×10^3	3.28×10^3	1.49×10^4	18%	82%
C3	6.62×10^2	5.78×10^3	2.9×10^5	1.62×10^4	5.78×10^3	4.30×10^3	5.20×10^3	08%	92%

2.8. Linear and Nonlinear Optical (NLO) Properties

To investigate the influence of excess electrons on triggering the NLO properties of studied polynuclear clusters, hyperpolarizability (β_o) and second hyperpolarizability (γ_o) are two crucial evaluation indices. The presence of excess electrons greatly increases the hyperpolarizability and second hyperpolarizability values, as shown in a number of studies [43,47–54]. We are interested in exploring the role of excess electrons in decreasing excitation energies, which ultimately escalates hyperpolarizabilities. The calculated linear and NLO parameters for the $C_3O[C(CN)_2]_2M_3$ (where $M = Li, Na$ and K) at CAM-B3LYP/6-311++g(d,p) clusters are given in Table 4. The α_o values lie in the range of 2.5×10^2 to 6.62×10^2 , and there is a slight increase with the increased size of alkali metals. These values show linear optical properties of polynuclear clusters, and the presence of polarizabilities is due to asymmetric electronic density distribution in these clusters.

The hyperpolarizability values of studied clusters range from 2.37×10^3 to 5.78×10^3 au, where the highest value is obtained for **C3**, while the lowest value is for the **C1** cluster. β_o values are increasing from Li to K metals within these clusters, which shows size dependence. It can be seen that electronic properties significantly contribute to hyperpolarizability response, and the larger the change in dipole moment, the higher the hyperpolarizabilities are. Thus, β_o values follow the increasing trend in these clusters, **C1** < **C2** < **C3**. Furthermore, the increased β_o values have a good match with reduced ionization potential and HOMO–LUMO gaps. The trend of size-dependent β_o is also shown in Figure 5.

In addition, the static second hyperpolarizability (γ_o) values are also calculated and lie in the range of 2.9×10^5 to 5.5×10^6 au (Table 4). Overall, γ_o values are significant where the highest value (5.5×10^6 au) is obtained for the **C1** cluster, while the lowest is for **C3**. It is found that, with the increased size of alkali metals, the γ_o values decrease slightly from Li to Na and then dramatically for K. These values follow decreasing trend of γ_o values in order of **C1** > **C2** > **C3**. The calculated significant γ_o values guarantee the superior NLO properties of polynuclear clusters. The calculated values of β_o and γ_o are quite significant as compared to previously reported M_2OCN superalkalis [47], M_2X (where $M = Li, Na$ and $X = F, Cl$) superalkali clusters, and lithium-based superalkalis Li_n ($n = 3, 5$, and 7) [55].

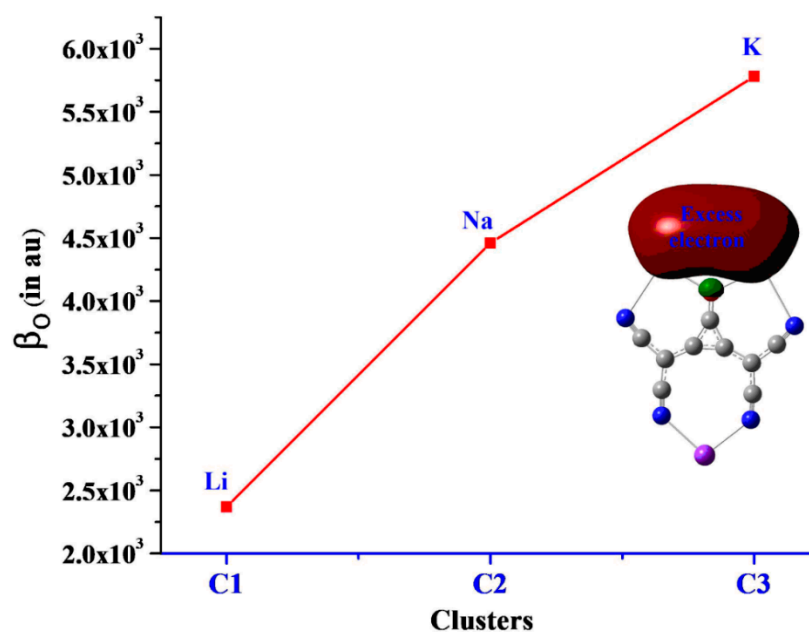


Figure 5. The representation of size-dependent hyperpolarizability (β_o).

Furthermore, the β_{vec} values are strongly correlated with total hyperpolarizability (β_o). The calculated β_{vec} values are given in Table 4. These values range from 2.37×10^3 to 5.78×10^3 au. The β_{vec} is the projection of hyperpolarizability on dipole moment vector and shows close resemblance β_o . However, good agreement between β_o and β_{vec} shows that the direction of the dipole moment vector and the projection of hyperpolarizability are in the same direction. The factor affecting β_{vec} values might be the same for β_o , where the highest β_{vec} values are obtained for higher-sized alkali metals (Table 4).

2.9. Scattering Hyperpolarizability (β_{HRS})

Density functional theory calculations have been carried out to find scattering hyperpolarizability (β_{HRS}), and values range from 1.34×10^3 to 1.62×10^4 au, where values are increasing steadily from the C1 to C3 cluster. The computed highest value is (1.62×10^4 au), found for C1 cluster, whereas the lowest value of 1.34×10^3 au is for the C1 cluster (Table 4). The β_{HRS} is the most viable parameter to calculate the hyperpolarizability of centrosymmetric molecules and clusters, even with zero change in dipole moment. There is an excellent agreement of β_{HRS} with β_o where the β_{HRS} show dependence on the size of alkali metals (M). The increased size of alkali metals (Li to K) favors the excellent electronic properties. Therefore, it also causes significantly enhanced β_{HRS} values. Additionally, average dipolar and octupolar hyperpolarizability, which are more prominent in C2 and C3 clusters, provide a notable contribution to β_{HRS} . Moreover, these clusters are of octupolar molecules, which can be seen by their highest octupolar contribution $\Phi\beta(j=3)$ of 92 % for C3 (Table 4).

2.10. Frequency Dependent NLO Properties

We theoretically examined the incident–frequency (ω) effect on the first and second hyperpolarizability at applied frequencies of 532 and 1064 nm. The frequency-dependent first hyperpolarizability $\beta(\omega)$ is calculated with the electro–optical Pockel’s effect (EOPE) and second harmonic generation (SHG), whereas the $\gamma(\omega)$ is expressed in terms of dc-Kerr effect and second harmonic generation (SHG). Overall, the dynamic hyperpolarizabilities values are higher than those of static hyperpolarizabilities. The significant EOPE effect $\beta(-\omega; \omega, 0)$ was observed for the C3 cluster at 532 nm, while its SHG value increased up to 1.7×10^6 au (Table 5). It can be demonstrated that the dynamic hyperpolarizabilities are higher at the smaller incident frequency ($\omega = 532$ nm) and slightly decreased at the higher

dispersion frequency (1064 nm). Strikingly, the $\beta(\omega)$ values are much more pronounced for the EOPE effect at both frequencies.

Table 5. Hyperpolarizability (β_0 in au), frequency-dependent hyperpolarizability $\beta(\omega)$ in terms of electro-optic-Pockel's effect (EOPE) $\beta(-\omega; \omega, 0)$ in au, and electric field induced second harmonic generation (EFSHG) $\beta(-2\omega; \omega, \omega)$ in au at $\omega = 532$ au.

Cluster	$\omega = 0$	$\omega = 532$ nm		$\omega = 1064$ nm	
	$\beta(0;0,0)$	$\beta(-\omega; \omega,0)$	$\beta(2-\omega;\omega,\omega)$	$\beta(-\omega; \omega,0)$	$\beta(-2\omega; \omega, \omega)$
C1	2.5×10^2	8.1×10^3	2.2×10^5	8.1×10^5	2.9×10^5
C2	5.0×10^2	1.0×10^5	4.2×10^5	2.7×10^6	1.6×10^5
C3	6.6×10^2	1.2×10^7	1.7×10^6	5.0×10^5	4.5×10^3

Furthermore, the $\gamma(\omega)$ values are higher than γ_0 , and the highest dc-Kerr value increased up to 2.6×10^9 au for C3 at 1064 nm (Table 6). The $\gamma(\omega)$ response becomes significant at the higher dispersion frequency (1064 nm), where SHG values are notable at both frequencies. The obtained higher values of the dc-Kerr effect reveal the nonlinear change in the refractive index of studied clusters. Hence, studied clusters have excellent NLO properties and can be used to design high-performance SHG devices.

Table 6. Static second hyperpolarizability (γ_0 in au), frequency-dependent second-hyperpolarizability $\gamma(\omega)$ in term of electro-optic-pockel's effect (EOPE) $\gamma(-\omega; \omega, 0)$ in au, and electric field-induced second harmonic generation (efshg) $\gamma(2-\omega; \omega, \omega)$ in au at $\omega = 532$ au.

Clusters	$\omega = 0$	$\omega = 532$ nm		$\omega = 1064$ nm	
	$\gamma(0;0,0,0)$	$\gamma(-\omega; \omega,0,0)$	$\gamma(-2\omega;\omega,\omega, \omega)$	$\gamma(-\omega; \omega,0,0)$	$\gamma(-2\omega; \omega, \omega, \omega)$
C1	5.5×10^6	3.0×10^8	6.0×10^7	1.0×10^6	1.2×10^8
C2	1.2×10^6	2.4×10^8	2.3×10^7	2.3×10^7	5.0×10^7
C3	2.9×10^5	4.9×10^7	1.7×10^8	2.6×10^9	2.0×10^9

3. Computational Details

All density functional theory (DFT) calculations are performed in the gas phase with Gaussian 09 software, whereas visualization is achieved using the GaussView 5.0 program [56,57]. Geometries of all polynuclear $C_3O[C(CN)_2]_2M_3$ (where M = Li, Na, and K) clusters are optimized at CAM-B3LYP/6-311++G(d,p) functionality [58]. The quantum mechanics-based Coulomb attenuating method (CAM-B3LYP) is a hybrid exchange-correlation functional that combines B3LYP's hybrid features with the CAM functional's long-range corrected parameter. It was found that this long-range corrected density functional substantially reduces the overestimation seen with conventional techniques and typically provides results that are comparable to those of coupled cluster calculations. Previous research has demonstrated that this method is well recognized for examining molecules and clusters, as well as for determining NLO properties [59,60]. Besides, the choice of a suitable basis set is crucial for obtaining reliable results. Thus, the CAM-B3LYP method with 6-311+G(d,p) split valence basis set is a reliable level of theory for geometry optimization and accuracy in results for electronic properties [61–65].

To determine whether the presented structures are true minima on the potential energy surface, frequency calculations are carried out. For thermodynamic stability, we calculated binding energy per atom for these clusters. Electronic stability and superalkali nature are validated through computed ionization energies (IE) and electron affinities (EA). To further explore the electronic properties, we performed frontier molecular orbital (FMO) analysis. Natural bonding orbitals (NBO) study is carried out to explore the charge distribution on

atoms within superalkali clusters [66]. The binding energy per atom (E_B) is given by the following relations:

$$E_B = [E_T(X) - E_A(X)^0]/n \quad (1)$$

where E_T is the total electronic energy of studied (X) superalkali clusters, $E_A(X)$ is the total energy of individual atoms within clusters, and n is the total number of atoms. The vertical ionization energy, electron affinity, and electrical conductivity (σ) can be represented by the equation:

$$VIE = E_X^+ - E_X^0 \quad (2)$$

$$VEA = E_X^0 - E_X^- \quad (3)$$

$$\sigma \propto \exp \frac{-E_G}{2kT} \quad (4)$$

where VIE and VEA are vertical ionization energies and electron affinities of studied clusters. In Equation (4), σ , E_G , k , and T represent the electrical conductivity, energy gap, Boltzmann constant, and temperature, respectively. To further explore the electronic properties of studied clusters, we also performed total density of state (TDOS) analysis at the same method by using the GaussSum software [67]. The following equation can be used to explain the molecules under the static electric field.

$$E(F) = E^0 - \mu_i F_i - \frac{1}{2} \alpha_{ij} F_i F_j - \frac{1}{6} \beta_{ijk} F_i F_j F_k - \frac{1}{24} \gamma_{ijkl} F_i F_j F_k F_l \dots \quad (5)$$

where F is an external applied electric field, F_i is the component of field along i direction, E^0 is the total energy of the superalkali clusters without a static electric field, and μ_i , α_{ij} , β_{ijk} , and γ_{ijkl} are dipole moment, polarizability, hyperpolarizability, and second-order hyperpolarizability, respectively. The mean dipole moment (μ_o), change in dipole moment ($\Delta\mu$), static polarizability (α_o), and static first hyperpolarizability (β_o) are calculated to illustrate the NLO response and associated responsible factors.

$$\alpha_o = 1/3 (\alpha_{xx} + \alpha_{yy} + \alpha_{zz}) \quad (6)$$

$$\beta_o = (\beta_x^2 + \beta_y^2 + \beta_z^2)^{1/2} \quad (7)$$

where $\beta_x = \beta_{xxx} + \beta_{xyy} + \beta_{xzz}$, $\beta_y = \beta_{yyy} + \beta_{yzz} + \beta_{yxx}$ and $\beta_z = \beta_{zzz} + \beta_{zxx} + \beta_{zyy}$.

$$\mu_o = (\mu_x^2 + \mu_y^2 + \mu_z^2)^{1/2} \quad (8)$$

To obtain absorption behaviors and excited state parameters of studied clusters, we performed TD-DFT simulations. We considered 30 states for getting excited states parameters. The Gaussian band shape and the absorption spectra were obtained by using the following relation, ϑ :

$$\varepsilon_o(\bar{\vartheta}) = \varepsilon_i^{max} \exp \left[- \left(\frac{\bar{\vartheta} - \bar{\vartheta}_i}{\sigma} \right)^2 \right] \quad (9)$$

where the i subscript represents the electronic excitation of interest. The other symbols in the equation have the following meanings:

- $\bar{\vartheta}_i$, shows the excitation energy (in wavenumbers) corresponding to the required electronic excitation in TD-DFT
- ε_i^{max} is the value of at the maximum of the band shape
- Sigma (σ) is a wavenumber representation of the standard deviation that is related to the simulated band's width.

The second static hyperpolarizability (γ_o) and the projection of hyperpolarizability on the dipole moment vector (β_{vec}) are also calculated for our studied superalkali clusters

at the same level of theory. Static second hyperpolarizability (γ_o) and vector part of hyperpolarizability (β_{vec}) are expressed as:

$$\langle \gamma \rangle = 1/5 (\gamma_{xxxx} + \gamma_{yyyy} + \gamma_{zzzz} + \gamma_{xxyy} + \gamma_{xxzz} + \gamma_{yyxx} + \gamma_{yyzz} + \gamma_{zzxx}) \quad (10)$$

$$\beta_{vec} = r \sum \mu^i \beta^i / |\mu| \quad (11)$$

Moreover, the molecular parameters relevant to electro-optical Pockel's effect (EOPE) and second harmonic generation (SHG) are calculated at externally applied frequencies (532 and 1064 nm).

4. Conclusions

In summary, we presented the geometric, electronic, and nonlinear optical properties of polynuclear carbon-based clusters at CAM-B3LYP/6-311++G(d,p) level. These clusters are thermodynamically stable, and their binding energies per atom range from -160.07 to -162.07 kcal mol $^{-1}$. The electronic stability and superalkali nature are characterized through calculated ionization potential (IP) and FMO analyses. Small ionization potential further suggests their superalkali nature. NBO charge analysis reveals excellent charge separation within clusters. The performed DOS analysis shows size-dependent electronic and conductive properties, where **C3** is a potential candidate. The significant first and second hyperpolarizabilities, up to 5.78×10^3 and 5.55×10^6 au, respectively, are calculated for the clusters. The β_o response shows dependence on the size of alkali metals. Furthermore, the absorption study shows their transparency in the deep-UV region for NLO applications and absorption at longer wavelengths. The significant scattering hyperpolarizability (β_{HRS}) value is (1.62×10^4), calculated for the **C3** cluster, where octupolar contribution to β_{HRS} is 92%. The dynamic first hyperpolarizability $\beta(\omega)$ is more pronounced for the EOPE effect at 532 nm, whereas SHG is more prominent for second hyperpolarizability $\gamma(\omega)$.

Supplementary Materials: The following supporting information can be downloaded at: <https://www.mdpi.com/article/10.3390/molecules28041827/s1>, Figure S1: DOS spectra of clusters; Table S1: Optimized geometries of clusters.

Author Contributions: I.B.: Methodology, Conceptualization, Funding acquisition; U.R.: Investigation, data handling; A.A.: Writing, Visualization; S.U.M.: Original draft preparation; N.S.S.: Software Validation, Editing; K.A.: Supervision and Reviewing. All authors have read and agreed to the published version of the manuscript.

Funding: This research was funded by the Deanship of Scientific Research, Vice Presidency for Graduate Studies and Scientific Research, King Faisal University, Saudi Arabia [Grant No. 2879].

Institutional Review Board Statement: Not applicable.

Informed Consent Statement: Not applicable.

Data Availability Statement: The author confirms that data supporting finding current study are available within article and in its supporting information. Raw data that supports the finding of this study are available from the corresponding author's upon request.

Acknowledgments: This work was supported by the Deanship of Scientific Research, Vice Presidency for Graduate Studies and Scientific Research, King Faisal University, Saudi Arabia [Grant No. 2879]. Also, thanks to the Higher Education Commission, Pakistan for the support [Grant No. 2981] and Universiti Brunei Darussalam [UBD/RSCH/1.4/FICBF(b)/2022/049].

Conflicts of Interest: The authors declare no conflict of interest.

Sample Availability: Not applicable.

References

1. Kanis, D.R.; Ratner, M.A.; Marks, T.J. Design and construction of molecular assemblies with large second-order optical nonlinearities. Quantum chemical aspects. *Chem. Rev.* **1994**, *94*, 195–242. [[CrossRef](#)]
2. He, G.S.; Tan, L.-S.; Zheng, Q.; Prasad, P.N. Multiphoton Absorbing Materials: Molecular Designs, Characterizations, and Applications. *Chem. Rev.* **2008**, *108*, 1245–1330. [[CrossRef](#)]
3. Dalton, L.R.; Steier, W.H.; Robinson, B.H.; Zhang, C.; Ren, A.; Garner, S.; Chen, A.; Londergan, T.; Irwin, L.; Carlson, B.; et al. From molecules to opto-chips: Organic electro-optic materials. *J. Mater. Chem.* **1999**, *9*, 1905–1920. [[CrossRef](#)]
4. Bredas, J.L.; Adant, C.; Tackx, P.; Persoons, A.; Pierce, B.M. Third-Order Nonlinear Optical Response in Organic Materials: Theoretical and Experimental Aspects. *Chem. Rev.* **1994**, *94*, 243–278. [[CrossRef](#)]
5. Kleinman, D.A. Nonlinear Dielectric Polarization in Optical Media. *Phys. Rev.* **1962**, *126*, 1977–1979. [[CrossRef](#)]
6. Xiao, D.; Bulat, F.A.; Yang, W.; Beratan, D.N. A Donor–Nanotube Paradigm for Nonlinear Optical Materials. *Nano Lett.* **2008**, *8*, 2814–2818. [[CrossRef](#)]
7. Palmer, S.; Sokolovski, S.G.; Rafailov, E.; Nabi, G. Technologic Developments in the Field of Photonics for the Detection of Urinary Bladder Cancer. *Clin. Genitourin. Cancer* **2013**, *11*, 390–396. [[CrossRef](#)]
8. Lee, S.; Park, J.; Jeong, M.; Kim, H.; Li, S.; Song, J.; Ham, S.; Jeon, S.; Cho, B. First hyperpolarizabilities of 1, 3, 5-tricyanobenzene derivatives: Origin of larger β values for the octupoles than for the dipoles. *ChemPhysChem* **2006**, *7*, 206–212. [[CrossRef](#)]
9. Noori, M.; Soroosh, M.; Baghban, H. Highly efficient self-collimation based waveguide for Mid-IR applications. *Photonics Nanostructures Fundam. Appl.* **2016**, *19*, 1–11. [[CrossRef](#)]
10. Clough, B.; Dai, J.; Zhang, X.-C. Laser air photonics: Beyond the terahertz gap. *Mater. Today* **2012**, *15*, 50–58. [[CrossRef](#)]
11. Xu, X.; Hu, C.-L.; Kong, F.; Zhang, J.-H.; Mao, J.-G.; Sun, J. ChemInform Abstract: Cs₂GeB₄O₉: A New Second-Order Nonlinear-Optical Crystal. *Inorg. Chem.* **2013**, *52*, 5831–5837. [[CrossRef](#)] [[PubMed](#)]
12. Liu, C.-G.; Guan, W.; Song, P.; Yan, L.-K.; Su, Z.-M. Redox-Switchable Second-Order Nonlinear Optical Responses of Push–Pull Monotetrathiafulvalene-Metalloporphyrins. *Inorg. Chem.* **2009**, *48*, 6548–6554. [[CrossRef](#)] [[PubMed](#)]
13. Chen, C.; Wu, Y.; Li, R. The development of new NLO crystals in the borate series. *J. Cryst. Growth* **1990**, *99*, 790–798. [[CrossRef](#)]
14. Kertész, M. Bond length alternation and energy gap in (CH)_x. Application of the intermediate exciton formalism. *Chem. Phys.* **1979**, *44*, 349–356. [[CrossRef](#)]
15. Arshad, Y.; Khan, S.; Hashmi, M.A.; Ayub, K. Transition metal doping: A new and effective approach for remarkably high nonlinear optical response in aluminum nitride nanocages. *New J. Chem.* **2018**, *42*, 6976–6989. [[CrossRef](#)]
16. Liu, Z.-B.; Zhou, Z.-J.; Li, Y.; Li, Z.-R.; Wang, R.; Li, Q.-Z.; Li, Y.; Jia, F.-Y.; Wang, Y.-F.; Li, Z.-J.; et al. Push–pull electron effects of the complexant in a Li atom doped molecule with electronegative character: A new strategy to enhance the first hyperpolarizability. *Phys. Chem. Chem. Phys.* **2010**, *12*, 10562–10568. [[CrossRef](#)]
17. Li, Z.; He, C.; Wang, Z.; Gao, Y.; Dong, Y.; Zhao, C.; Chen, Z.; Wu, Y.; Song, W. Ethylenediamine-modified graphene oxide covalently functionalized with a tetracarboxylic Zn(II) phthalocyanine hybrid for enhanced nonlinear optical properties. *Photochem. Photobiol. Sci.* **2016**, *15*, 910–919. [[CrossRef](#)]
18. Maury, O.; Le Bozec, H. Molecular Engineering of Octupolar NLO Molecules and Materials Based on Bipyridyl Metal Complexes. *Accounts Chem. Res.* **2005**, *38*, 691–704. [[CrossRef](#)]
19. Hatua, K.; Nandi, P.K. Beryllium-Cyclobutadiene Multidecker Inverse Sandwiches: Electronic Structure and Second-Hyperpolarizability. *J. Phys. Chem. A* **2013**, *117*, 12581–12589. [[CrossRef](#)]
20. Li, X.-H.; Zhang, L.; Zhang, X.-L.; Ni, B.-L.; Li, C.-Y.; Sun, W.-M. Designing a new class of excess electron compounds with unique electronic structures and extremely large non-linear optical responses. *New J. Chem.* **2020**, *44*, 6411–6419. [[CrossRef](#)]
21. Zhong, R.-L.; Xu, H.-L.; Muhammad, S.; Zhang, J.; Su, Z.-M. The stability and nonlinear optical properties: Encapsulation of an excess electron compound LiCN^{•-} Li within boron nitride nanotubes. *J. Mater. Chem.* **2011**, *22*, 2196–2202. [[CrossRef](#)]
22. Ahsan, A.; Ayub, K. Adamantane based alkaline earths with excellent nonlinear optical response and ultraviolet transparency. *Opt. Laser Technol.* **2020**, *129*, 106298. [[CrossRef](#)]
23. Casida, M.E.; Jamorski, C.; Casida, K.C.; Salahub, D.R. Molecular excitation energies to high-lying bound states from time-dependent density-functional response theory: Characterization and correction of the time-dependent local density approximation ionization threshold. *J. Chem. Phys.* **1998**, *108*, 4439–4449. [[CrossRef](#)]
24. Mulliken, R.S. Rydberg States and Rydbergization. *Acc. Chem. Res.* **1976**, *9*, 7–12. [[CrossRef](#)]
25. Zhong, R.-L.; Xu, H.-L.; Li, Z.-R.; Su, Z.-M. Role of Excess Electrons in Nonlinear Optical Response. *J. Phys. Chem. Lett.* **2015**, *6*, 612–619. [[CrossRef](#)]
26. Zhong, R.; Xu, H.; Sun, S.; Qiu, Y.; Su, Z. The Excess Electron in a Boron Nitride Nanotube: Pyramidal NBO Charge Distribution and Remarkable First Hyperpolarizability. *Chem.—Eur. J.* **2012**, *18*, 11350. [[CrossRef](#)]
27. Chen, W.; Li, Z.-R.; Wu, D.; Li, Y.; Sun, C.-C.; Gu, F.L. The Structure and the Large Nonlinear Optical Properties of Li@Calix[4]pyrrole. *J. Am. Chem. Soc.* **2005**, *127*, 10977–10981. [[CrossRef](#)]
28. Ma, F.; Li, Z.; Xu, H.; Li, Z.; Li, Z.; Aoki, Y.; Gu, F. Lithium salt electronegative with an excess electron pair—A class of nonlinear optical molecules for extraordinary first hyperpolarizability. *J. Phys. Chem. A* **2008**, *112*, 11462–11467. [[CrossRef](#)] [[PubMed](#)]
29. Li, B.; Peng, D.; Gu, F.L.; Zhu, C. A nonlinear optical switch induced by an external electric field: Inorganic alkaline–earth alkali. *RSC Adv.* **2019**, *9*, 16718–16728. [[CrossRef](#)]

30. Ahsan, A.; Ayub, K. Extremely large nonlinear optical response and excellent electronic stability of true alkaline earthides based on hexaammine complexant. *J. Mol. Liq.* **2019**, *297*, 111899. [[CrossRef](#)]
31. Ayub, K.; Ahsan, F. Transition metalides based on facially polarized all-cis-1, 2, 3, 4, 5, 6-hexafluorocyclohexane—a new class of high performance second order nonlinear optical materials. *Phys. Chem. Chem. Phys.* **2023**, *25*, 4732–4737.
32. Sun, W.-M.; Li, X.-H.; Wu, D.; Li, Y.; He, H.-M.; Li, Z.-R.; Chen, J.-H.; Li, C.-Y. A theoretical study on superalkali-doped nanocages: Unique inorganic electrides with high stability, deep-ultraviolet transparency, and a considerable nonlinear optical response. *Dalton Trans.* **2016**, *45*, 7500–7509. [[CrossRef](#)] [[PubMed](#)]
33. Kim, J.; Ichimura, A.; Huang, R.; Redko, M.; Phillips, R.; Jackson, J.; Dye, J. Crystalline Salts of Na- and K- (Alkalides) that Are Stable at Room Temperature. *J. Am. Chem. Soc.* **1999**, *121*, 10666–10667. [[CrossRef](#)]
34. Ichimura, A.S.; Dye, J.L.; Cambor, M.A.; Villaescusa, L.A. Toward Inorganic Electrides. *J. Am. Chem. Soc.* **2002**, *124*, 1170–1171. [[CrossRef](#)] [[PubMed](#)]
35. Hou, J.; Jiang, D.; Qin, J.; Duan, Q. Alkaline-earthide: A new class of excess electron compounds $\text{Li-C}_6\text{H}_6\text{F}_6\text{-M}$ ($\text{M} = \text{Be, Mg and Ca}$) with extremely large nonlinear optical responses. *Chem. Phys. Lett.* **2018**, *711*, 55–59. [[CrossRef](#)]
36. Sun, W.-M.; Li, X.-H.; Wu, J.; Lan, J.-M.; Li, C.-Y.; Wu, D.; Li, Y.; Li, Z.-R. Can Coinage Metal Atoms Be Capable of Serving as an Excess Electron Source of Alkalides with Considerable Nonlinear Optical Responses? *Inorg. Chem.* **2017**, *56*, 4594–4600. [[CrossRef](#)] [[PubMed](#)]
37. Gutsev, G.; Boldyrev, A. DVM $X\alpha$ calculations on the electronic structure of “superalkali” cations. *Chem. Phys. Lett.* **1982**, *92*, 262–266. [[CrossRef](#)]
38. Sikorska, C.; Gaston, N. $\text{N}_4\text{Mg}_6\text{M}$ ($\text{M} = \text{Li, Na, K}$) superalkalis for CO_2 activation. *J. Chem. Phys.* **2020**, *153*, 144301. [[CrossRef](#)]
39. Saedi, L.; Dodangi, M.; Mohammadpanaardakan, A.; Eghtedari, M. Superalkali–Superhalogen Complexes as Versatile Materials for Hydrogen Storage: A Theoretical Study. *J. Clust. Sci.* **2019**, *31*, 71–78. [[CrossRef](#)]
40. Park, H.; Meloni, G. Activation of Dinitrogen with a Superalkali Species, Li_3F_2 . *ChemPhysChem* **2018**, *19*, 256–260. [[CrossRef](#)]
41. Giri, S.; Behera, S.; Jena, P. Superalkalis and Superhalogens as Building Blocks of Supersalts. *J. Phys. Chem. A* **2014**, *118*, 638–645. [[CrossRef](#)] [[PubMed](#)]
42. Percec, V.; Won, B.C.; Peterca, M.; Heiney, P.A. Expanding the Structural Diversity of Self-Assembling Dendrons and Supramolecular Dendrimers via Complex Building Blocks. *J. Am. Chem. Soc.* **2007**, *129*, 11265–11278. [[CrossRef](#)] [[PubMed](#)]
43. Ullah, F.; Kosar, N.; Ayub, K.; Mahmood, T. Superalkalis as a source of diffuse excess electrons in newly designed inorganic electrides with remarkable nonlinear response and deep ultraviolet transparency: A DFT study. *Appl. Surf. Sci.* **2019**, *483*, 1118–1128. [[CrossRef](#)]
44. Sajid, H.; Ayub, K.; Mahmood, T. Exceptionally high NLO response and deep ultraviolet transparency of superalkali doped macrocyclic oligofuran rings. *New J. Chem.* **2020**, *44*, 2609–2618. [[CrossRef](#)]
45. Srivastava, A.; Misra, N. Nonlinear optical behavior of Li_nF ($n = 2\text{--}5$) superalkali clusters. *J. Mol. Model.* **2015**, *21*, 1–5. [[CrossRef](#)] [[PubMed](#)]
46. Srivastava, A.K.; Misra, N. M_2X ($\text{M} = \text{Li, Na; X} = \text{F, Cl}$): The smallest superalkali clusters with significant NLO responses and electride characteristics. *Mol. Simul.* **2016**, *42*, 981–985. [[CrossRef](#)]
47. Ahsin, A.; Ayub, K. Theoretical investigation of superalkali clusters M_2OCN and M_2NCO (where $\text{M} = \text{Li, Na, K}$) as excess electron system with significant static and dynamic nonlinear optical response. *Optik* **2020**, *227*, 166037. [[CrossRef](#)]
48. Ahsin, A.; Ayub, K. Extremely large static and dynamic nonlinear optical response of small superalkali clusters $\text{NM}_3\text{M}'$ ($\text{M, M}' = \text{Li, Na, K}$). *J. Mol. Graph. Model.* **2021**, *109*, 108031. [[CrossRef](#)]
49. Li, X.-H.; Zhang, X.-L.; Chen, Q.-H.; Zhang, L.; Chen, J.-H.; Wu, D.; Sun, W.-M.; Li, Z.-R. Coinage metalides: A new class of excess electron compounds with high stability and large nonlinear optical responses. *Phys. Chem. Chem. Phys.* **2020**, *22*, 8476–8484. [[CrossRef](#)]
50. Ahsin, A.; Ali, A.; Ayub, K. Alkaline earth metals serving as source of excess electron for alkaline earth metals to impart large second and third order nonlinear optical response; a DFT study. *J. Mol. Graph. Model.* **2020**, *101*, 107759. [[CrossRef](#)] [[PubMed](#)]
51. Ahsin, A.; Ayub, K. Remarkable electronic and NLO properties of bimetallic superalkali clusters: A DFT study. *J. Nanostructure Chem.* **2021**, *12*, 529–545. [[CrossRef](#)]
52. Ahsin, A.; Ayub, K. Zintl based superatom P_7M_2 ($\text{M} = \text{Li, Na, K \& Be, Mg, Ca}$) clusters with excellent second and third-order nonlinear optical response. *Mater. Sci. Semicond. Process.* **2021**, *134*, 105986.
53. Ahsin, A.; Ayub, K. Superalkali-based alkalides $\text{Li}_3\text{O}@[12\text{-crown-4}]\text{M}$ (where $\text{M} = \text{Li, Na, and K}$) with remarkable static and dynamic NLO properties; A DFT study. *Mater. Sci. Semicond. Process.* **2021**, *138*, 106254. [[CrossRef](#)]
54. Ahsin, A.; Ayub, K. Oxacarbon superalkali $\text{C}_3\text{X}_3\text{Y}_3$ ($\text{X} = \text{O, S}$ and $\text{Y} = \text{Li, Na, K}$) clusters as excess electron compounds for remarkable static and dynamic NLO response. *J. Mol. Graph. Model.* **2021**, *106*, 107922. [[CrossRef](#)]
55. Ahsin, A.; Ayub, K. Theoretical investigation of lithium-based clusters Li_n (where $n = 3, 5, 7$) with remarkable electronic and frequency-dependent NLO properties. *Eur. Phys. J. Plus* **2022**, *137*, 803. [[CrossRef](#)]
56. Frisch, M.J.; Trucks, G.W.; Schlegel, H.B.; Scuseria, G.E.; Robb, M.A.; Cheeseman, J.R.; Scalmani, G.; Barone, V.; Petersson, G.A.; Nakatsuji, H.; et al. *Gaussian 09*; Gaussian, Inc.: Wallingford, CT, USA, 2009.
57. Dennington, R.; Keith, T.A.; Millam, J.M. *GaussView*, 6th ed.; Semichem Inc.: Shawnee Mission, KS, USA, 2009.
58. Grein, F. Influence of diffuse and polarization functions on the second-order Møller–Plesset optimized dihedral angle of biphenyl. *Theor. Chem. Accounts* **2003**, *109*, 274–277. [[CrossRef](#)]

59. Okuno, K.; Shigeta, Y.; Kishi, R.; Miyasaka, H.; Nakano, M. Tuned CAM-B3LYP functional in the time-dependent density functional theory scheme for excitation energies and properties of diarylethene derivatives. *J. Photochem. Photobiol. A Chem.* **2012**, *235*, 29–34. [[CrossRef](#)]
60. Kobayashi, R.; Amos, R.D. The application of CAM-B3LYP to the charge-transfer band problem of the zincbacteriochlorin–bacteriochlorin complex. *Chem. Phys. Lett.* **2006**, *420*, 106–109. [[CrossRef](#)]
61. Bravo-Pérez, G.; Garzón, I.; Novaro, O. Ab initio study of small gold clusters. *J. Mol. Struct. THEOCHEM* **1999**, *493*, 225–231. [[CrossRef](#)]
62. Marchetti, O.; Werner, H.-J. Accurate Calculations of Intermolecular Interaction Energies Using Explicitly Correlated Coupled Cluster Wave Functions and a Dispersion-Weighted MP2 Method. *J. Phys. Chem. A* **2009**, *113*, 11580–11585. [[CrossRef](#)] [[PubMed](#)]
63. Castet, F.; Rodriguez, V.; Pozzo, J.-L.; Ducasse, L.; Plaquet, A.; Champagne, B. Design and Characterization of Molecular Nonlinear Optical Switches. *Accounts Chem. Res.* **2013**, *46*, 2656–2665. [[CrossRef](#)] [[PubMed](#)]
64. Maroulis, G. Quantifying the performance of conventional DFT methods on a class of difficult problems: The interaction (hyper)polarizability of two water molecules as a test case. *Int. J. Quantum Chem.* **2011**, *112*, 2231–2241. [[CrossRef](#)]
65. Karamanis, P.; Maroulis, G.; Pouchan, C. Molecular geometry and polarizability of small cadmium selenide clusters from all-electron ab initio and Density Functional Theory calculations. *J. Chem. Phys.* **2006**, *124*, 71101. [[CrossRef](#)] [[PubMed](#)]
66. Reed, A.E.; Weinstock, R.B.; Weinhold, F. Natural population analysis. *J. Chem. Phys.* **1985**, *83*, 735–746. [[CrossRef](#)]
67. Allouche, A.-R. Gabedit-A graphical user interface for computational chemistry softwares. *J. Comput. Chem.* **2010**, *32*, 174–182. [[CrossRef](#)] [[PubMed](#)]

Disclaimer/Publisher’s Note: The statements, opinions and data contained in all publications are solely those of the individual author(s) and contributor(s) and not of MDPI and/or the editor(s). MDPI and/or the editor(s) disclaim responsibility for any injury to people or property resulting from any ideas, methods, instructions or products referred to in the content.